



Manilkara zapota (L.) P. Royen Leaf Extract Derived Silver Nanoparticles Induce Apoptosis in Human Colorectal Carcinoma Cells Without Affecting Human Lymphocytes or Erythrocytes

V. S. Shaniba¹ · Ahlam Abdul Aziz¹ · P. R. Jayasree² · P. R. Manish Kumar¹

Received: 3 September 2018 / Accepted: 22 January 2019 / Published online: 8 March 2019
© Springer Science+Business Media, LLC, part of Springer Nature 2019

Abstract

Plant-derived synthesis of silver nanoparticles (AgNPs) has found wide biomedical applications including cancer cure. This report deals with biosynthesis of silver nanoparticles (MZLAgNPs) employing leaf extracts of *Manilkara zapota* (L.) under optimized conditions. Characterization of MZLAgNPs using UV-Vis spectroscopy, FTIR, XRD, and FESEM analyses revealed that the particles were predominantly spherical averaging 24 nm in size. Their cellular effects were assessed by MTT assay, fluorescence, and scanning electron microscopy of cells stained with propidium iodide, acridine orange/ethidium bromide, and annexin V-FITC to visualize signs of apoptosis. Evaluation of cell proliferation by clonogenic assay, wound healing ability by scratch assay and cell cycle distribution by flow-cytometry was also carried out. Apoptosis-related gene expressions were analyzed by RTq-PCR and western blot analysis. MZLAgNPs selectively inhibited growth of colorectal carcinoma HCT116, HeLa, and non-small lung carcinoma A549 cells, dose-dependently with IC₅₀ concentrations of 8, 16, and 29 µg/mL respectively, following 72-h treatment, without affecting growth of normal human lymphocytes and erythrocytes. Apoptosis induction was observed by fluorescence and scanning electron microscopy. Overproduction of reactive oxygen species (ROS), reduction of mitochondrial membrane potential, upregulation of apoptotic-related genes - PUMA, cas-3, cas-8, cas-9, and BAX, expression of caspase 3, and occurrence of PARP cleavage were observed in MZLAgNPs/cisplatin treated cells. Taken together, our results clearly demonstrate the therapeutic potential of biogenic MZLAgNPs as an effective agent for killing colorectal carcinoma cells by apoptosis induction.

Keywords Silver nanoparticles · *Manilkara zapota* · Colorectal carcinoma · Apoptosis

Introduction

Nanoparticles (NPs) comprise of clusters of atoms in the size range of 1–100 nm. Gold, silver, and platinum have been used mostly for the synthesis of stable dispersions

Electronic supplementary material The online version of this article (<https://doi.org/10.1007/s12011-019-1653-6>) contains supplementary material, which is available to authorized users.

✉ P. R. Manish Kumar
manishramakrishnan@rediffmail.com; prmanishkumar@uoc.ac.in

V. S. Shaniba
Shanibavsn@gmail.com

¹ Recombinant DNA Laboratory, Department of Biotechnology, University of Calicut, Malappuram, Kerala 673635, India

² School of Health sciences, University of Calicut, Malappuram, Kerala 673635, India

of nanoparticles useful in many areas including optoelectronics, functional biology, drug delivery, antimicrobial, and biosensors [1]. Chemical and physical means of nanoparticle synthesis, though popular, entail use of hazardous chemicals, large amounts of energy, and generate harmful wastes [2, 3]. These adversely affect the environment and are technically laborious and expensive. A ‘greener’ alternative for biogenic synthesis of nanoparticles exploits natural products such as sugars, biopolymers [4], microorganisms [5], and plant extracts [6]. The cellular constituents therein are believed to play a key role as bioreductants in the conversion of metal ions to nanoparticles as well as provide capping agents to stabilize them. The use of plant extracts has been found to be relatively more advantageous over microbial systems for large scale production of biogenic nanoparticles since maintenance of aseptic conditions for microbial cultures is not industrially feasible [7].

A plethora of studies have confirmed anticancer activities of biogenic gold, silver, copper, titanium, zinc, and iron prepared from different bio-sources [8, 9]. Among these, silver nanoparticles have gained greater popularity and acceptability due to their antibacterial, antifungal, larvicidal, anti-parasitic properties as well as industrial applications [10]. The cytotoxicity of silver nanoparticles (AgNPs) is dependent on parameters such as particle size, surface area/reactivity, distribution pattern and cell-type specificity [11], though the exact mechanism of their action is not yet fully understood. The proposed mechanisms involve generation of reactive oxygen species (ROS), causation of mitochondrial damage, induction of sub-G₁ arrest [12], up-regulation of p53 protein, caspase-3 expression [13], and inhibition of vascular endothelial growth factor-induced activities [14]. The physico-chemical and biological traits of these particles make them excellent drug-delivery vehicles which are increasingly becoming popular in clinical use. The use of surface-modified nano-scale liposomes/lipid-micelles to deliver hydrophilic and hydrophobic anticancer drugs as well as siRNA formulations is a promising development in cancer therapy sometimes referred to as nano-oncology within the broader discipline termed as nanomedicine [15, 16].

Manilkara zapota (L.) P. Royen or *Achras sapota*, commonly known as sapodilla (Family *Sapotaceae*) is an evergreen tree cultivated throughout India, originally native to Mexico and Central America [17]. The plant parts have found wide use in traditional medicine. Fruits, flowers, and leaves have been used against cough, colds, bronchitis, diarrhea, and dysentery [18–20] whilst seeds and bark have been used as aperients, diuretic tonic, astringent, and febrifuge [21, 22]. The fruit known as chickoo or sapota, a natural energy booster enriched in fructose/sucrose and a rich source of dietary fiber, minerals, and vitamins is recommended for prevention of micronutrient malnutrition [23]. Besides flavonoids and polyphenols, the plant contains phytochemicals such as saponins, triterpenoids, dihydromyricetin, myricitrin, quercetin, catechins, and gallic acid which are known to possess anti-inflammatory, antimicrobial, antioxidant, analgesic, and spermicidal activities [24, 25]. In an earlier study, Ma et al. [26] reported isolation of two phenolic antioxidant compounds—methyl 4-O-galloylchlorogenate and 4-O-galloylchlorogenic acid which were found to be cytotoxic against two colorectal cancer cell lines—HCT 116 and SW 480 with IC₅₀ values ranging within 100–200 μ M. A subsequent study revealed the presence of lupeol acetate, oleanolic acid, apigenin-7-O-a-L-rhamnoside, myricetin-3-O-a-L-rhamnoside, caffeic acid, *n*-triacontane, *n*-octacosane, and two sterols— β -sitosterol and stigmasterol [27]. Later, yet another compound, erythrodiol, with potent antitumour activity in mice, was isolated from *M. zapota* leaf [28]. Likewise, methanolic extract of the fruit also was reported to significantly inhibit tumor progression in mice [29].

In this context, the present study aimed at green synthesis of silver nanoparticles (AgNPs) employing leaf-extracts of *Manilkara zapota* (MZL) and their physico-chemical characterization. This is the first report on the evaluation of the anticancer potential of MZLAgNPs on human cancer cell lines and normal human peripheral blood lymphocytes and erythrocytes.

Materials and Methods

Chemicals and Reagents

M. zapota leaves were collected from Malappuram district of Kerala State. Silver nitrate (AgNO₃), Tris base, glycine, acridine orange (AO), ethidium bromide (EtBr), potassium bromide, and heparin were purchased from SRL Pvt. Ltd., (Mumbai, India). 5-Bromo-4-chloro-3-indolyl phosphate/nitro blue tetrazolium (BCIP/NBT), dimethyl sulfoxide (DMSO), dichloro-dihydro-fluorescein-diacetate (DCFH-DA), rhodamine 123, annexin V- FITC apoptosis detection kit, propidium iodide, TRI reagent, and crystal violet were purchased from Sigma-Aldrich (USA). SYBR Green PCR Master Mix was purchased from TAKARA (Japan). Anti-caspase-3, anti-PARP anti-actin antibodies were purchased from Cell Signaling Technology, USA. Goat anti-rabbit IgG-alkaline phosphatase (ALP)-conjugate, goat anti-mouse IgG-ALP-conjugate, RNase inhibitor, oligo (dT)18 primer, DTT, and reverse transcriptase enzyme were purchased from Bangalore Genei (Merck Life Sciences, Mumbai, India). Fetal bovine serum (FBS) and 0.25% Trypsin-EDTA were obtained from Gibco (Thermo Fisher Scientific, USA). Bovine serum albumin (BSA), Dulbecco's Modified Eagle's Medium (DMEM), HiKaryo XL™ RPMI medium, and MTT (3-(4, 5-dimethylthiazol-2-yl)-2, 5-diphenyltetrazolium bromide) were purchased from HiMedia Laboratories Pvt. Ltd., Mumbai, India.

Maintenance of Cancer Cell Lines

Three human carcinoma cells—colorectal HCT 116, cervical HeLa, and non-small lung alveolar A549 cells were obtained from Govt. of India—National Centre for Cell Sciences (NCCS), Pune, for the study. The cells were grown as a monolayer in DMEM medium supplemented with 10% FBS and 100 U/mL each of penicillin-streptomycin and incubated at 37 °C in a humidified 5% CO₂ atmosphere.

Biosynthesis of Silver Nanoparticles

The dried leaves of *M. zapota* (MZL) were cut into small pieces and powdered finely. For extract preparation, 10 g of leaf powder was weighed and mixed with 200 mL milli-Q water and boiled for 15 min. After cooling, MZL was filtered

through layers of muslin cloth and Whatman No. 1 filter paper and stored at 4 °C in the refrigerator. Effective AgNPs synthesis was achieved by optimizing parameters such as (i) volume of MZL ranging from 2.0 to 10.0 mL, (ii) concentration of silver metal ion ranging from 0.5 to 5.0 mM, (iii) temperature ranging from 37 to 100 °C, (iv) pH ranging from 4.0 to 9.0, and (v) time of incubation ranging from 0 to 2.5 h. The reaction mixtures were periodically monitored in the range of 200–700 nm using a UV-Vis spectrophotometer to detect formation of MZLAGNPs.

Characterization of Silver Nanoparticles

Following visual detection of the yellowish brown color associated with the formation of silver nanoparticles and confirmation of the characteristic λ_{\max} , the reaction mixture was centrifuged at 12000 rpm for 20 min and the resultant pellet was resuspended in milli-Q water and lyophilized (Scanvac- coolsafe). To characterize the bioactive constituents present in the extract, the freeze-dried powder was pelletized with potassium bromide (KBr) powder and subjected to Fourier-transform infrared spectroscopic (FTIR) analysis using Jasco 4100 at a wavelength ranging from 4000 to 400 cm^{-1} . For X-ray diffraction (XRD) studies, the dried MZLAGNPs were coated on XRD grid and the spectrum was recorded using a Rigaku miniflex X-ray diffractometer with $\text{CuK}\alpha$ radiation (40 kV, 15 mA). The average size of particles was determined using field emission electron microscope (FESEM), Horiba S46600.

Assessment of Cytotoxicity by MTT and Trypan Blue Dye Exclusion Assay

The cytotoxicity of MZLAGNPs was evaluated by MTT assay. All three cell types were individually seeded (1×10^4 cells/well) into 96-well tissue culture plates and incubated for 24 h. The cells were then exposed to different concentrations of MZLAGNPs (2.5–70 $\mu\text{g}/\text{mL}$) or to the chemotherapeutic drug cisplatin (positive control) for 24, 48, and 72 h. Following addition of MTT (500 $\mu\text{g}/\text{mL}$), the cells were then incubated further for another 3 h at 37 °C. The formazan crystals formed were then dissolved in 150 μL of DMSO for optical density measurements at 620 nm using an ELISA plate reader (Multiscan EX, Thermo Scientific, USA). The difference of absorbance between the treated and untreated control groups was used to determine cell viability [30]. The cell line HCT 116 which displayed the highest sensitivity to MZLAGNPs in terms of IC_{50} concentration was selected for all assays employed for further detailed probing.

Trypan blue dye exclusion assay was performed to evaluate the effect of MZLAGNPs on HCT 116 cell viability. For this, cells were seeded at a density of 1.5×10^5 cells/well into 12-

well plate followed by nanoparticle treatment for 24 h. Following a PBS wash, cells were stained with PBS containing 0.4% trypan blue and counted using hemocytometer. The unstained cells were regarded as live whilst the blue cells were counted as dead cells [31].

Clonogenic Assay

Cells were plated at a density of 5×10^2 cells per well in 6-well plates and treated with MZLAGNPs/cisplatin; untreated cells were also maintained as controls. Following 48 h of incubation and a change of growth medium, the cells were subjected to a further incubation period of 7 days. Colonies were then stained using crystal violet (0.5%w/v) and counted manually [32].

Viability (%)

$$= \frac{\text{Colonies counted in control plate}}{\text{Colonies counted in treated plate}} \times 100$$

Cell Migration Assay

Cells were seeded in 35-mm culture dish and incubated until a monolayer was formed. Linear wounds were made by scratching with a microtip and the detached cells were removed with a PBS wash. Each culture dish was then treated with either MZLAGNPs or cisplatin. Cell movement into the wound area was monitored and photographed at 0, 12, and 24 h using a light microscope. The average migration rates were calculated as following:

Cell motility(%)

$$= \frac{\text{The wound width at 0 h} - \text{the wound width at 12/24 h}}{\text{The wound width at 0 h}} \times 100$$

Cytomorphological Observations

The control, MZLAGNPs, and cisplatin-treated cells were trypsinized and washed with ice-cold PBS. The cytomorphological changes were observed under phase-contrast inverted microscope and FESEM. Briefly, separate aliquots of cells were fixed with 4% glutaraldehyde followed by PBS wash. It was then dehydrated by passing through ascending graded acetone series (75–85–100%) and the dried cells were coated with gold [33] and observed under a Hitachi SU6600 scanning electron microscope. The control and treated cells were stained with Hoechst 33258 and their nuclear morphology was examined under a fluorescence microscope. To ascertain induction of apoptosis, cells were dual-stained with acridine orange/ethidium bromide (AO-EtBr) and viewed under a fluorescence microscope (40 \times magnification) to determine percentage apoptosis.

Comet Assay

Genotoxicity of MZLAgNPs was evaluated by alkaline gel electrophoresis. The control and MZLAgNP-treated cells were washed with PBS and subjected to comet assay as described by [34]. Following electrophoresis, the slides were washed with neutralization buffer, stained with ethidium bromide (10 µg/mL), and observed under a fluorescence microscope.

Study of Intracellular ROS, Phosphatidylserine (PS) Externalization, and Mitochondrial Membrane Potential (MMP)

Intracellular ROS was studied using the dye DCFH-DA-based assay. Both the control and treated cells were incubated with 10 µM DCFH-DA at 37 °C for 30 min in the dark and then washed twice with PBS prior to microscopic examination [35]. PS externalization was determined by FITC-labeled annexin V/PI according to the manufacturer's protocol (Sigma, USA). The depletion of MMP, an early marker of apoptosis, was evaluated by incubating the treated and control cells with lipophilic cationic dye Rhodamine 123 (10 µg/mL) for 30 min. Cells were then harvested and washed twice with PBS [36]. In all cases, the cells were mounted on slides and their images were captured using fluorescence microscopy.

Reverse Transcription Quantitative PCR (RT-qPCR) Analysis

The relative levels of apoptosis-related gene expressions were evaluated by RT-qPCR employing six sets of gene-specific primers—PUMA, caspase-3, caspase-8, caspase-9, Bcl-2, and Bax [34, 37]—the sequences of which are given in Table 1. Total RNA isolated from treated and control cells using TRI reagent was used to synthesize cDNA. Briefly, a 5 µL reaction containing 0.5 µL of oligo dT (100 ng/µL) and 1.0 µL of 0.5 µg/µL RNA was incubated at 65 °C for 10 min and placed on ice. To this, added 1.0 µL of 10 mM dNTP mix, 2.0 µL of 10× M-MLV reverse transcriptase buffer, 1.0 µL of M-MLV reverse transcriptase, 0.5 µL of RNasin, 0.5 µL DTT (20 mM), and made up to 10 µL with sterile nuclease-free water. The reaction mixture was incubated at 37 °C for 1 h, heated to 95 °C for 10 min and stored at −20 °C until use. The real-time PCR was performed on an Illumina Eco™ Real Time system (San Diego) using SYBR Green PCR master Mix according to the manufacturer's protocol. Relative expression levels were calculated using $\Delta\Delta C_t$ method with GAPDH as internal reference gene.

Table 1 Primers used in RT-qPCR assay

Gene	Primer sequence
PUMA	Forward: 5'GACCTCAACGACAGTACGA3 Reverse: 5'GAGATTGTACAGGACCCTCCA3'
Caspase 3	Forward: 5'TGGCATACTCCACAGCACCTGGTTA3' Reverse: 5'CATGGCACACAAAGCGACTGGATGAA3'
Caspase 8	Forward: 5'CATCCAGTCACTTTGCCAGA3' Reverse: 5'GCATCTGTTTCCCCATGTTT3'
Caspase 9	Forward: 5'TTCCCAGTTTTGTTTCTG3' Reverse: 5'CCTTTCACCGAAACAGCATT3'
Bax	Forward: 5'GCCACCAGCCTGTTTGAG3' Reverse: 5'CTGCCACCCAGCCACCC3'
Bcl-2	Forward: 5'TATAAGCTGTCGCAGAGGGGCTA3' Reverse: 5'GTACTCAGTCATCCACAGGGCGAT3'
GAPDH	Forward: 5AATCCCATCACCATCTTCCA3 Reverse: 5'CCTGCTTCACCACCTTCTTG3'

Western Blot Analysis

Western blotting was performed as previously described [38] to investigate expression levels of apoptosis related proteins. The control, MZLAgNPs, and cisplatin-treated cells were washed with cold PBS and lysed in RIPA buffer. Cells were carefully scraped and incubated on ice for 30 min. The total cellular lysate was centrifuged at 10,000×g for 10 min to clear cell debris and protein concentration was measured using Bradford method. Protein samples (50 µg) were electrophoresed on a 12.5% SDS-PAGE gel and then transferred onto a polyvinylidene fluoride (PVDF) membrane. Membranes were washed with Tris-buffered saline Tween-20 (TBST), blocked with 5% skimmed milk for 1 h at room temperature and incubated overnight at 4 °C separately with rabbit-derived primary antibodies (dilution 1:1000) against caspase-3, PARP, and a mouse monoclonal antibody for β actin acting as a loading control to detect house-keeping function. Following a wash with TBST, the membranes were incubated with ALP-conjugated secondary antibody (1:2000 dilution) for 1 h at room temperature. Following a subsequent wash with TBST, the blots were exposed to BCIP/NBT solution to visualize the immunostained polypeptides.

Assessment of MZLAgNPs Cytotoxicity on Normal Human Cells

Cellular toxicity of MZLAgNPs was assessed employing human peripheral blood lymphocyte cultures (hPBLs). Isolated lymphocytes (10⁵ cells/mL) were cultured in HiKaryo XL™ RPMI medium supplemented with phytohemagglutinin. MTT assay was carried out essentially as described earlier. The OD_{620nm} was measured and the difference of absorbance between the treated and untreated control

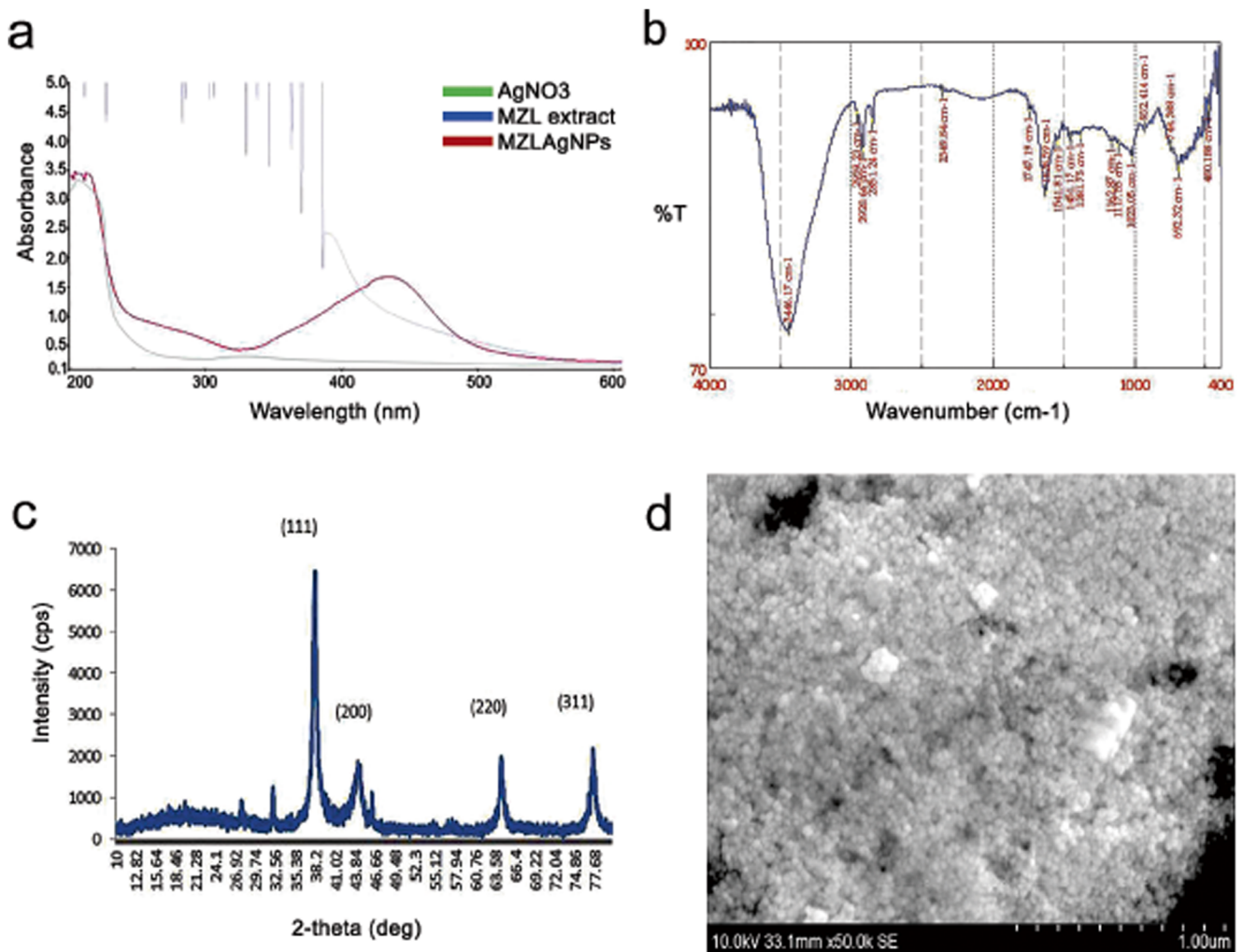


Fig. 1 a UV-visible spectrum, b FTIR spectrum, c X-ray diffraction analysis, and d FESEM image of MZLAgNPs

cells was used to determine cell viability. Hemolytic assay was performed using human blood from healthy donors. The red blood cells (RBCs) were isolated by centrifugation at 1500 rpm for 5 min followed by four washes with sterile PBS. Erythrocytes were then incubated with varying concentrations (50–200 $\mu\text{g/mL}$) of both MZLAgNPs and cisplatin separately for 90 min at 37 $^{\circ}\text{C}$. The samples were then centrifuged at 3000 rpm for 10 min and the absorbance of the supernatants were measured at 543 nm using a

spectrophotometer to monitor hemolysis. Percent hemolysis (H) was calculated by the formula,

$$H = \frac{(OD_S - OD_0)}{(OD_{100} - OD_0)} \times 100$$

where OD_S , OD_0 , and OD_{100} denote optical densities of experimental, negative (PBS), and positive (water) controls respectively [39].

Table 2 IC_{50} values of MZLAgNPs obtained for three human cancer cell lines

Cell lines tested	IC_{50} obtained on exposure to MZLAgNPs for different time periods		
	24 h ($\mu\text{g/mL}$)	48 h ($\mu\text{g/mL}$)	72 h ($\mu\text{g/mL}$)
HCT 116	25 \pm 2	23 \pm 3	8 \pm 3
HeLa	54 \pm 1	38 \pm 2	16 \pm 2
A549	84 \pm 1	44 \pm 1	29 \pm 3

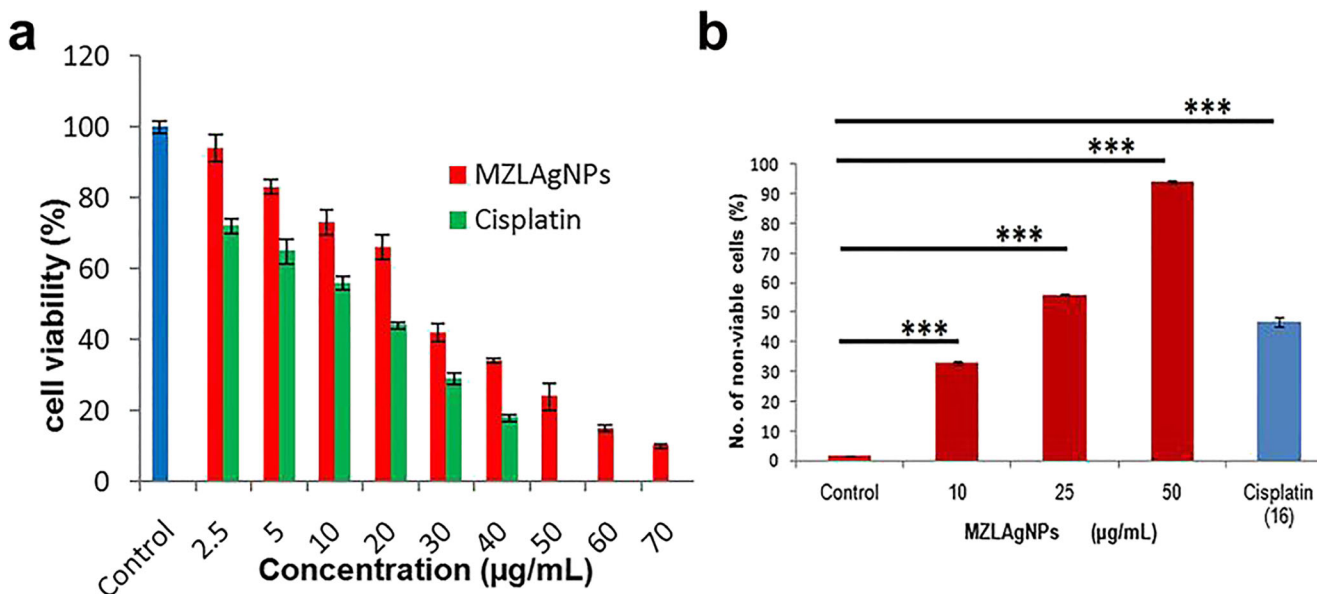


Fig. 2 Effect of MZLAgNPs on HCT 116 cells. **a** Cell viability was measured by MTT method after 24 h treatment. **b** The percentage of non-viable cells was evaluated by trypan blue dye exclusion method.

Data shown as mean ± SD of three independent experiments (*** $P \leq 0.001$, ** $P \leq 0.01$, * $P \leq 0.05$)

Statistical Analysis

The data are expressed as the mean ± SD from three independent experiments. Results were analyzed for significance by one-way ANOVA using SPSS software version 20.0. Differences with $P < 0.05$ were considered significant. Asterisks (*) were used to identify the level of significance (* $P \leq 0.05$, ** $P \leq 0.01$, *** $P \leq 0.001$).

Results

Optimum Conditions for MZLAgNPs Biosynthesis

Using a trial and error method, conditions were optimized for green synthesis of MZLAgNPs. A 2.0 ml aliquot of the aqueous MZL extract was mixed with 98.0 ml of 1.0 mM AgNO_3 (pH 4.0). Incubation of the mixture at 90 °C for 30 min

Fig. 3 a Clonogenic capacity in MZLAgNP/cisplatin-treated HCT 116 cells as measured by colony-forming assay; colonies were stained with crystal violet (control, 10, 25, 50 µg/mL and cisplatin, 16 µg/mL). **b** The number of colonies in MZLAgNP-treated HCT cells were significantly reduced as compared with control (*** $P \leq 0.001$)

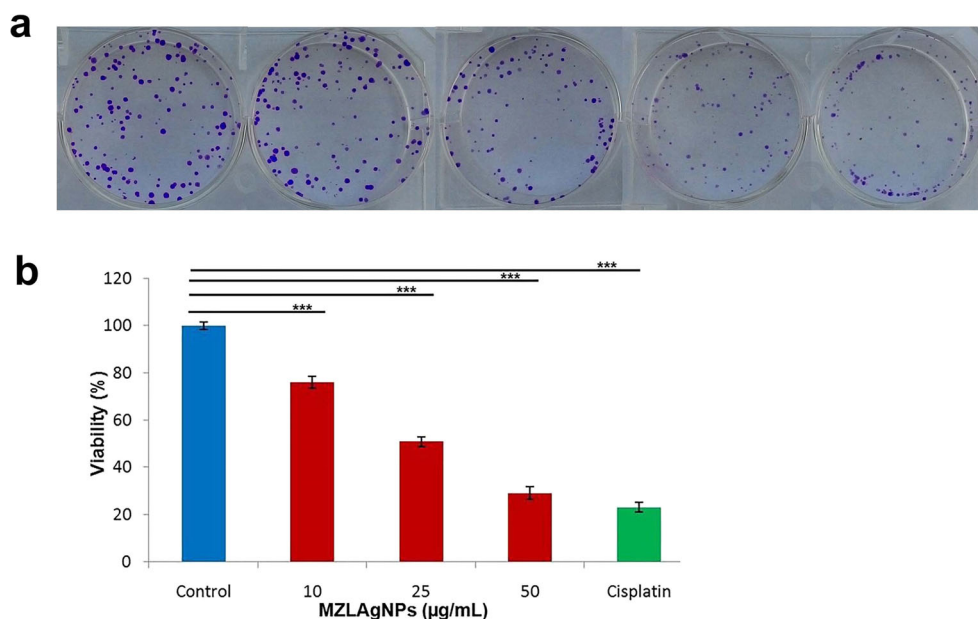


Fig. 4 a Cell migration assay showed that MZLAGNPs inhibited the migration of HCT 116 cells (control, 10, 25, 50 $\mu\text{g}/\text{mL}$ and cisplatin, 16 $\mu\text{g}/\text{mL}$). **b** Reduction in scratched area (wound closure) due to cell migration was measured and expressed in percentage relative to control. Data shown as mean \pm SD of three independent experiments

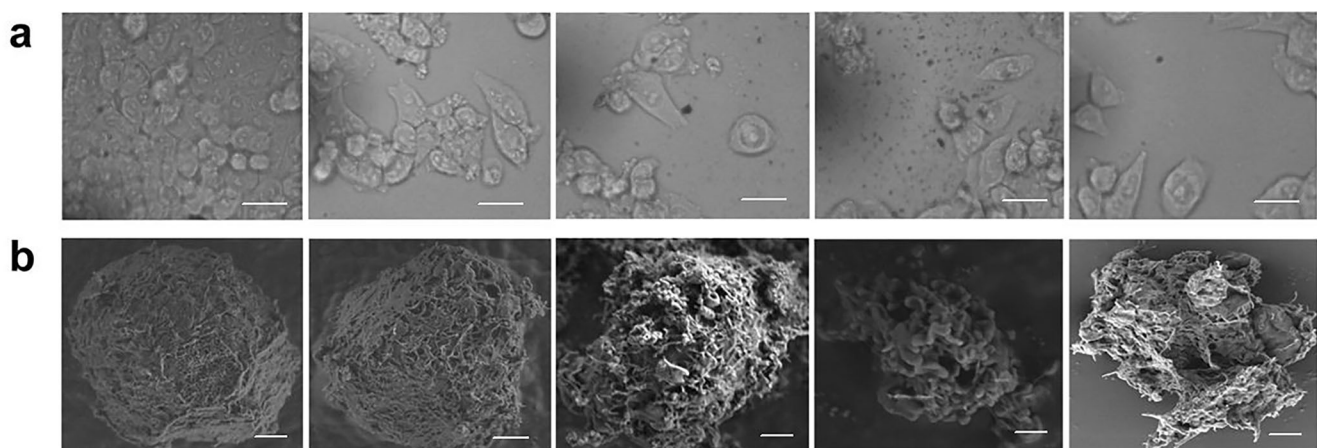
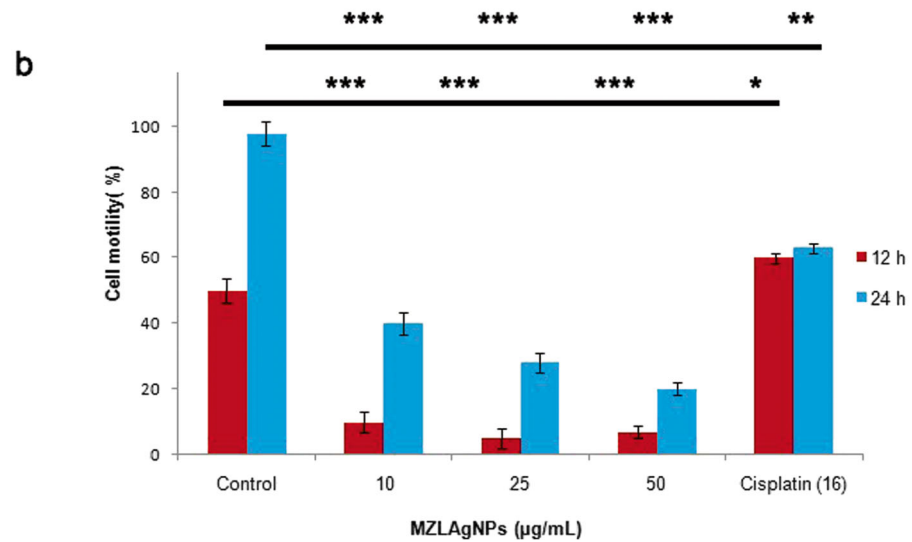
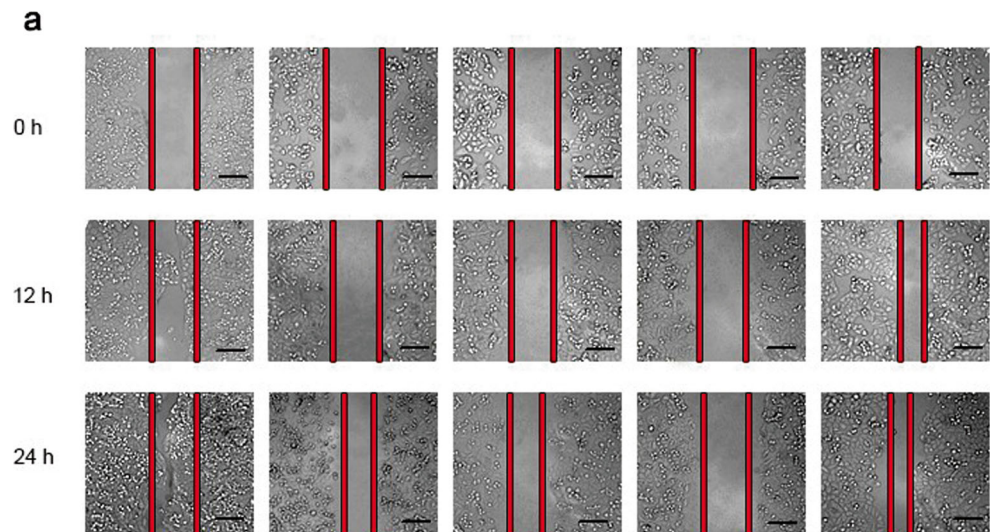


Fig. 5 Morphological changes in HCT 116 cells after 24 h treatment. **a** Light microscopic images of MZLAGNPs (10, 25, 50 $\mu\text{g}/\text{mL}$) and cisplatin-16 $\mu\text{g}/\text{mL}$ (scale bars 20 μm). **b** Field emission scanning

electron microscopic images of control, MZLAGNPs (10, 25, 50 $\mu\text{g}/\text{mL}$) and cisplatin, 16 $\mu\text{g}/\text{mL}$ (scale bars 2 μm)

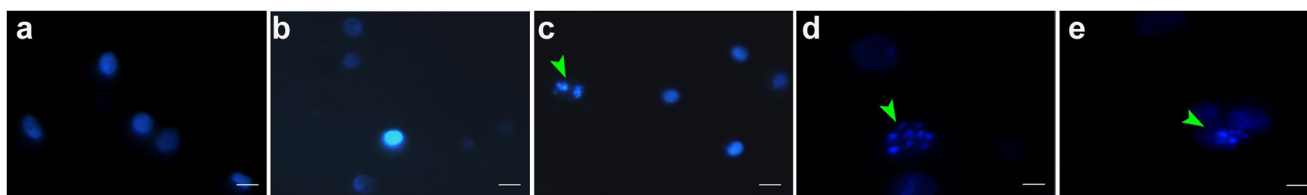


Fig. 6 Fluorescence microscopy images of HCT 116 cells stained with Hoechst 33258, arrow heads indicate apoptotic nuclear condensation and DNA fragmentation **a** control, **b** 10 μg/mL, **c** 25 μg/mL, **d** 50 μg/mL of MZLAGNPs, and **e** cisplatin, 16 μg/mL (scale bars 20 μm)

resulted in the generation of biogenic MZLAGNPs. The characteristic absorption spectrum of silver nanoparticles as evidenced by the formation of brown color was obtained at 430 nm for MZLAGNPs as a consequence of surface plasmon resonance (SPR) of AgNPs (Fig. 1a).

Characterization of MZLAGNPs

FTIR spectroscopy was carried out to examine the presence of bioreducing and capping agents present in the leaf extract presumably adsorbed/associated with the biogenic MZLAGNPs. The results showed an intensive peak at 3446 cm⁻¹ corresponding to O–H stretching of alcohols and phenols. Peaks at 2959 cm⁻¹, 2920 cm⁻¹, and 2851 cm⁻¹ represented C–H binding whilst peaks at 1747 cm⁻¹ represented carbonyl groups (C=O) and peaks at 1023 cm⁻¹ indicated C–O bond. Further, peaks at 1541 cm⁻¹ and 1451 cm⁻¹ indicated N–O asymmetric stretching and peaks at 744 cm⁻¹ and 692 cm⁻¹ represented C–Cl stretch (Fig. 1b). The characteristic peaks observed in X-ray diffraction pattern of MZLAGNPs confirmed the presence of

silver nanoparticles (Fig. 1c). The XRD peaks at 38.05°, 44.2°, 64.39°, and 77.26° corresponded to the (111), (200), (220), and (311) planes of face-centered cubic phase. The average crystal size was found to be 24 nm as calculated by Debye Scherrer’s formula. Morphometric measurements observed under FESEM showed predominantly spherical-shaped particles of varying sizes ranging from 10 to 80 nm size (Fig. 1d).

Cytotoxicity of MZLAGNPs on Human Cancer Cell Lines

An MTT assay-based cytotoxicity assessment of MZLAGNPs was carried out against three human cancer cell lines—HCT 116, A549, and HeLa cells. Biogenic AgNPs showed the highest cytotoxicity against HCT 116 cells in comparison to that of HeLa and A549 as evidenced by the decrease in the IC₅₀ value from 25 to 8 for 24- and 72-h treatment respectively (Table 2). The dose-dependent cell viability of HCT 116 cells exposed to MZLAGNPs/cisplatin for the concentration range tested is given in Fig. 2a; the IC₅₀ concentration determined

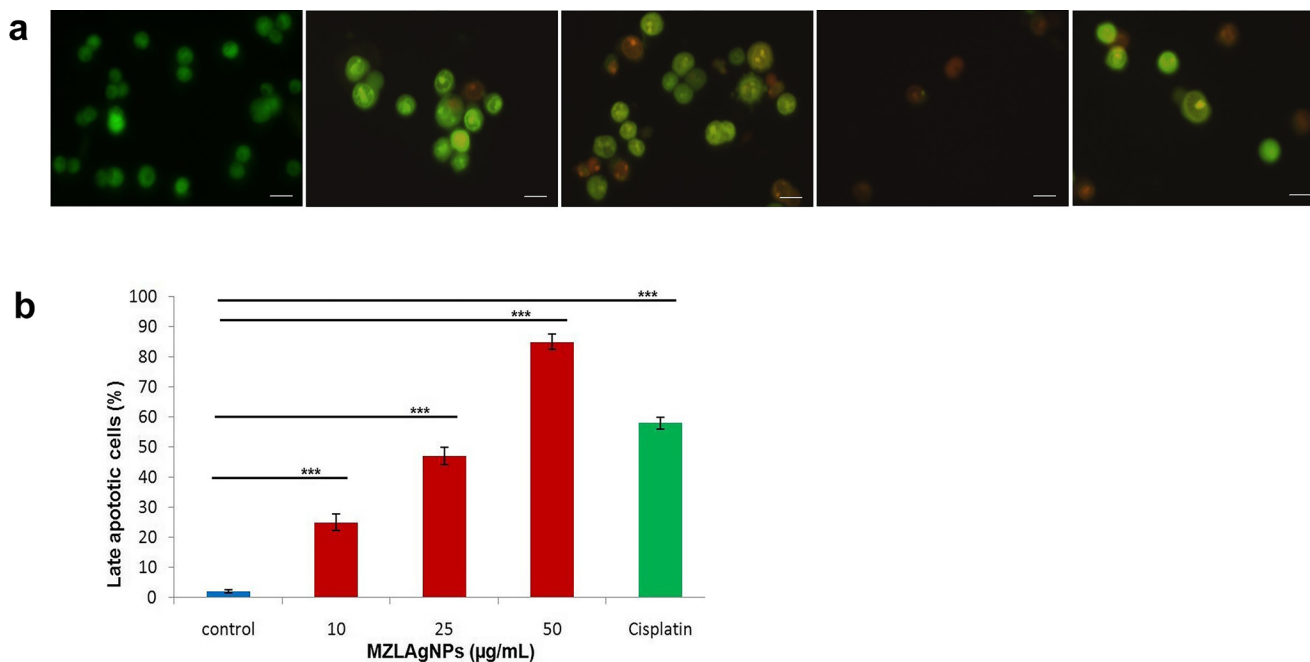


Fig. 7 Apoptotic changes of AO/EtBr stained MZLAGNPs treated HCT 116 cells. **a** Fluorescence microscopy images of control, MZLAGNPs (10, 25, 50 μg/mL) and cisplatin, 16 μg/mL. **b** Quantitative analysis of late

apoptotic cells (scale bars 20 μm). Data shown as mean ±SD of three independent experiments (***) $P \leq 0.001$

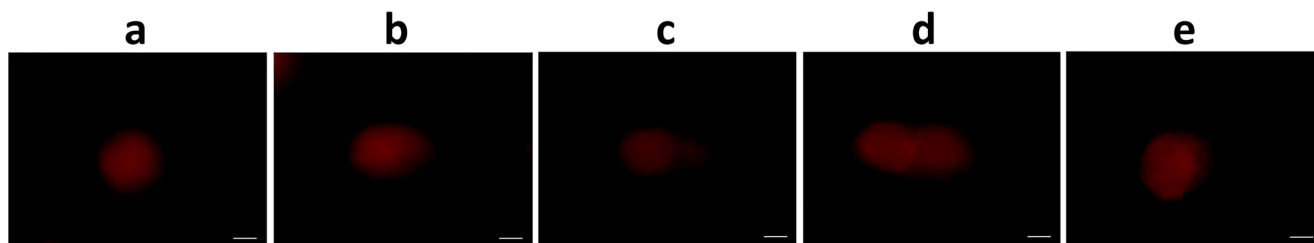


Fig. 8 Detection of DNA damage by alkaline comet assay in HCT 116 cells treated with MZLAGNPs/cisplatin for 24 h. **a** Control, **b** 10 µg/mL, **c** 25 µg/mL, **d** 50 µg/mL of MZLAGNPs, **e** cisplatin, 16 µg/mL (scale bars 20 µm)

for cisplatin being 16 µg/ml (MTT assay results obtained for HeLa and A549 cells are provided in the supplementary data Fig. 1). The results of the trypan blue dye exclusion method corroborated well with that of MTT assay (Fig. 2b). Since HCT 116 cells showed the highest sensitivity towards MZLAGNP-based cytotoxicity, these cells were employed for all subsequent detailed experiments to evaluate the cellular effects and mechanism of action of these biogenic nanoparticles.

Clonogenic Assay

Clonogenic assay was performed to determine the effect of MZLAGNPs on HCT 116 cell's reproductive ability. A concentration-dependent reduction in colony formation

capability, compared to that of control cells, was observed following treatment with MZLAGNPs in a dose-dependent manner indicative of effective suppression of growth and proliferation of the cells (Fig. 3a, b).

Wound Healing Assay

The effects of MZLAGNPs/cisplatin on HCT 116 cell migration for 12–24 h duration were evaluated through wound healing assay. The results revealed that nanoparticle treated HCT 116 cells displayed the highest inhibitory effect on cell migration, much more than that observed in cisplatin treated cells when compared to untreated cells (Fig. 4a, b).

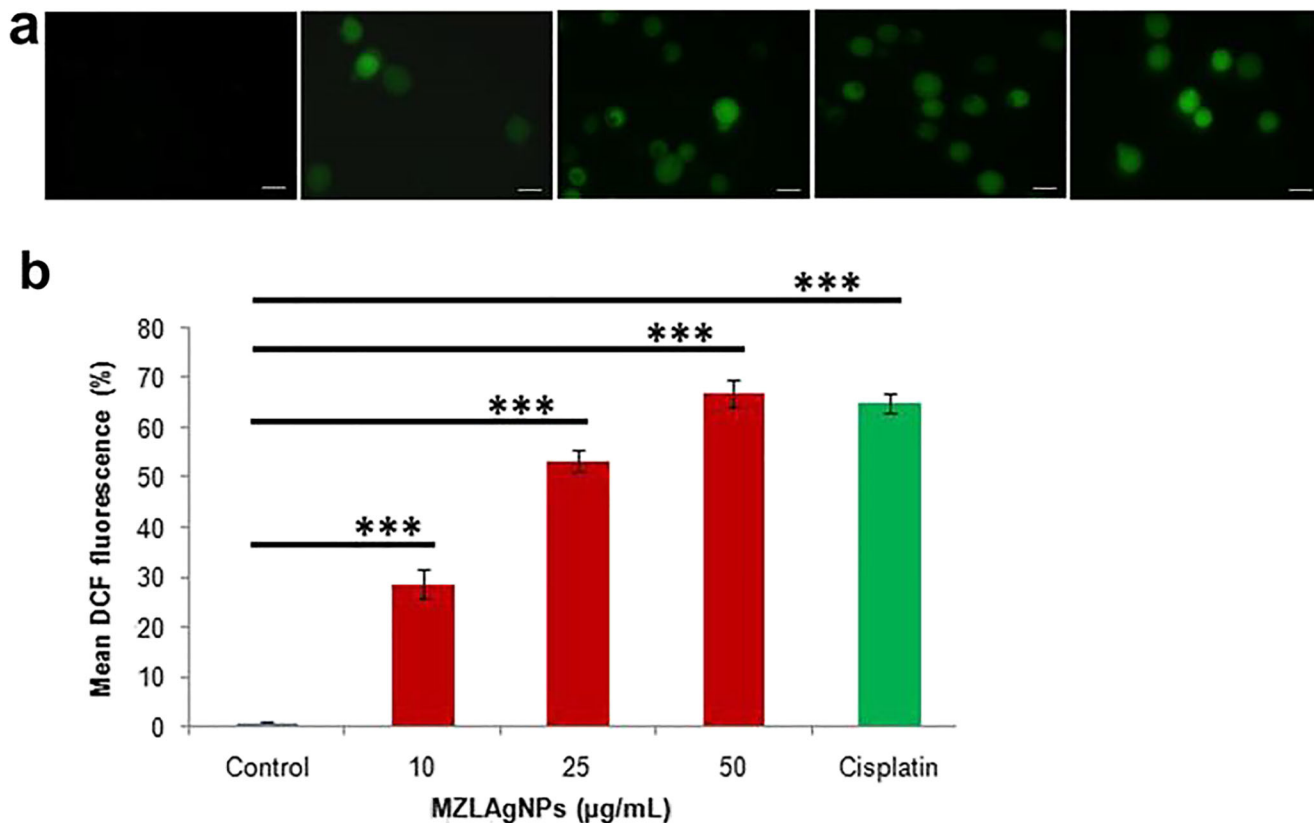


Fig. 9 Measurement of cellular ROS in MZLAGNP-treated HCT 116 cells **a** fluorescent microscopic images of control, MZLAGNPs (10 µg/mL, 25 µg/mL, 50 µg/mL) and cisplatin, 16 µg/mL (scale bars 20 µm). **b**

Mean fluorescent intensity of cells stained with ROS indicator DCFH-DA. Data shown as mean ± SD of three independent experiments (***) $P \leq 0.001$

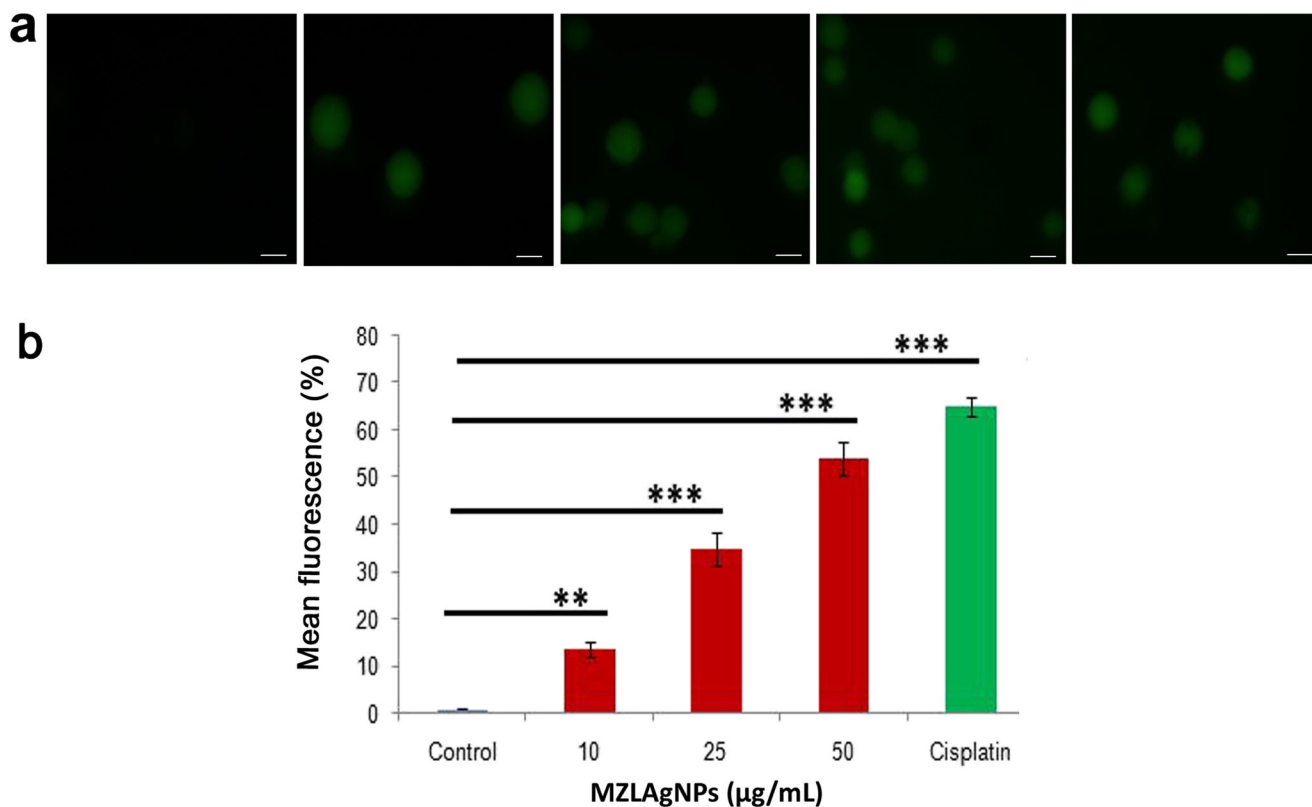


Fig. 10 Measurement of mitochondrial membrane potential in MZLAgNP-treated HCT 116 cells. **a** Fluorescence microscopy images of control, MZLAgNPs (10 µg/mL, 25 µg/mL, 50 µg/mL) and cisplatin,

16 µg/mL (scale bars 20 µm). **b** Mean fluorescent intensity of cells stained with Rhodamine 123. Data shown as mean ± SD of three independent experiments (*** $P \leq 0.001$, ** $P \leq 0.01$)

MZLAgNPs Causes Cytomorphological Alterations

The first and most readily noticeable effect following exposure of cells to toxic materials is the alteration in cell shape or morphology in a monolayer culture. Light and scanning electron microscopy of MZLAgNPs/cisplatin-treated cells showed distinct cellular morphological alterations such as cell shrinkage, extensive membrane blebbing with restricted cell spreading patterns. The control cells appeared normal as irregular confluent aggregates of rounded and polygonal cells. Dose-dependent cellular changes were apparent in micrographs of treated cells obtained with both of the techniques (Fig. 5a, b).

To confirm whether the cytotoxic effects induced by MZLAgNPs involved apoptotic induction, staining with Hoechst 33258 was carried out to check for presence of condensed chromatin. Apoptosis related nuclear condensation and fragmentation were observed resulting from intense uptake of stain in such regions (Fig. 6). Following dual staining with AO-EtBr, viable cells were characterized by possession of uniformly bright green nuclei, early/late apoptotic cells with bright green and orange area of condensed or fragmented chromatin and necrotic cells with uniformly bright orange nuclei (Fig. 7a). A quantitative analysis based on cell counts showed a dose-dependent induction of apoptosis leading to

85% cell death at the highest test concentration of 50 µg/mL of MZLAgNPs (Fig. 7b).

Genotoxicity of MZLAgNPs

DNA damaging potential of MZLAgNPs was assessed by the comet assay. A concentration-dependent increase in the tail moment was observed in the treated cells which was found to be absent in the untreated controls (Fig. 8). A comet-like tail implied presence of damaged DNA strands trailing behind an intact nucleus during electrophoresis.

Effect of MZLAgNPs on Intracellular ROS, MMP, and PS Externalization

The use of DCFH-DA for indirect estimation of intracellular ROS concentration involves measuring intracellular generation of hydrogen peroxide. This probe is cell permeable and is hydrolyzed intracellularly to the DCFH carboxylate anion which is retained in the cell. Oxidation of DCFH results in the formation of dihydrofluorescein which emits fluorescence directly proportional to the amount of ROS generated. HCT 116 cells incubated with MZLAgNPs showed a dose-dependent increase in ROS production compared to that observed in controls (Fig. 9).

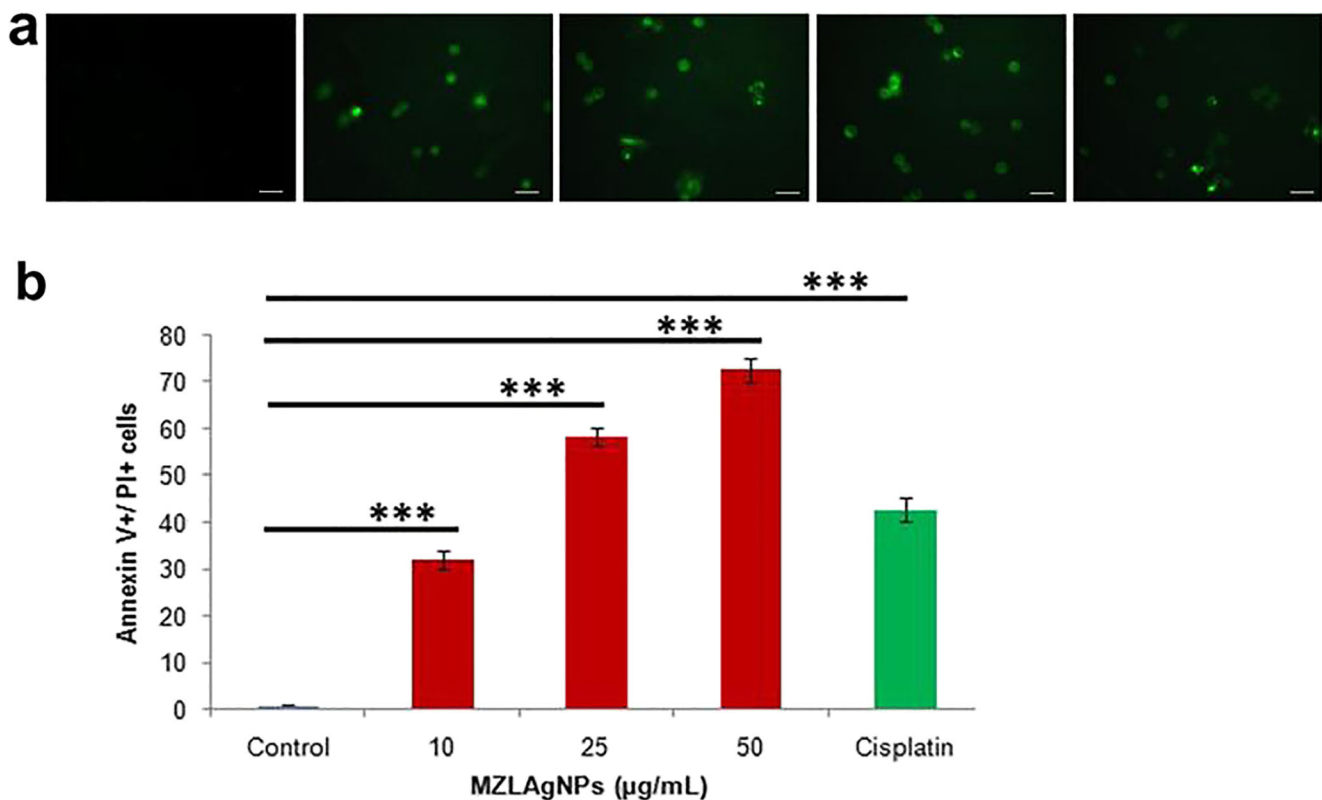


Fig. 11 Detection of apoptosis by annexin V-FITC/PI staining in MZLAgNP-treated HCT 116 cells. **a** Fluorescence microscopy images of control, MZLAgNPs (10 µg/mL, 25 µg/mL, 50 µg/mL) and cisplatin,

16 µg/mL (scale bars 20 µm). **b** Quantitative analysis of annexin V+/PI+ cells. Data shown as mean ± SD of three independent experiments (***) $P \leq 0.001$

Likewise, depletion of MMP, an early marker of apoptosis, was observed employing mitochondria-specific and voltage-dependent, fluorescent lipophilic cationic dye, Rhodamine123 in MZLAgNPs/cisplatin-treated cells (Fig. 10). Annexin V-FITC staining carried out to determine the extent and mode of cell death induced by MZLAgNPs revealed a dose-dependent increase in the number of annexin V positive HCT 116 cells (Fig. 11).

RTq-PCR Analysis

Expression levels of apoptotic related genes such as p53-upregulated modulator of apoptosis (PUMA), caspase-3, caspase-8, caspase-9, Bcl-2, and Bax were also determined for studying MZLAgNP-induced changes in transcriptional profile. Exposure to MZLAgNPs resulted in more than threefold increase in expression of caspase-3, caspase-8, and PUMA compared with the corresponding transcript levels observed in cisplatin-treated positive controls. Overall, transcript quantitation by RTq-PCR technique clearly demonstrated induction of apoptosis through upregulation of PUMA, caspase-3, caspase-8, caspase-9, and Bax and down regulation of anti-apoptotic Bcl-2 expression (Fig. 12).

Western Blot Analysis

Detection of cleaved PARP protein as well as caspase-3, major apoptotic proteins, on western blots have provided unequivocal proof of apoptosis induction by MZLAgNPs via mitochondria-mediated intrinsic pathway (Fig. 13). However, within the concentration range tested, a dose-dependent increase in the expression of these proteins commensurate with the increased transcript levels detected in RTq-PCR analysis could not be observed.

Effects of MZLAgNPs on Human Lymphocytes (hPBLs) and Erythrocytes

The effect of varying concentrations of MZLAgNPs (10, 30, 60, and 80 µg/mL)/cisplatin on proliferation of hPBLs was determined by MTT assay. The results clearly indicated that treatment with nanoparticles at IC_{50} concentration neither affected lymphocyte proliferation nor was toxic to them (Fig. 14) contrary to the toxicity of cisplatin. Further, the extent of hemolysis observed in erythrocytes (Fig. 15) at the IC_{50} concentration apparently did not cause any harmful effect on human erythrocytes.

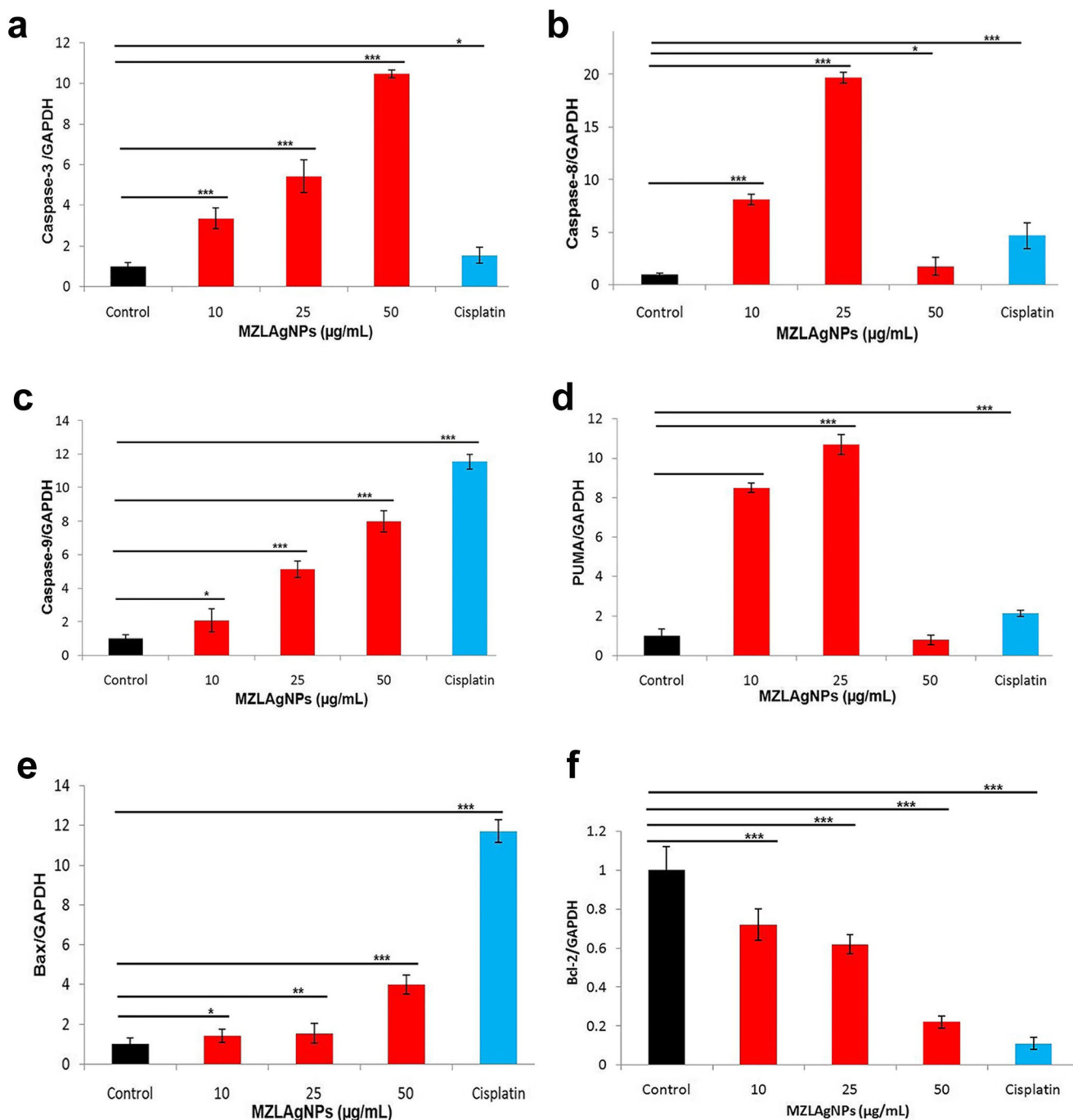


Fig. 12 The relative quantification of mRNA expression of apoptosis related genes using RTq-PCR in HCT 116 cells treated with MZLAgNPs and cisplatin (16 µg/mL). **a** Caspase-3. **b** Caspase-8. **c**

Caspase-9. **d** PUMA. **e** Bax. **f** Bcl-2. Data shown as mean ± SD of three independent experiments (** $P \leq 0.001$, ** $P \leq 0.01$, * $P \leq 0.05$)

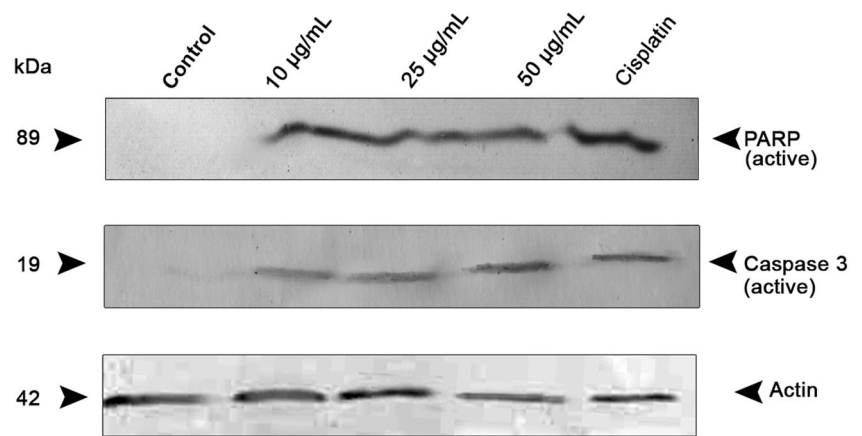
Discussion

Metal nanoparticles are multifaceted agents with a variety of applications particularly in nanomedicine for highly sensitive diagnostic assays, biological labeling, and radiotherapy enhancement including drug/gene delivery [40]. The present study involved an environmentally benign method utilizing *Manilkara zapota* leaf extract for synthesis of nanoparticles

averaging 24 nm in size based on SPR phenomenon [41]. FTIR spectrum clearly showed the presence of active phytoconstituents like phenolics, flavonoids, alcohol, ketone, and carboxylic acid functional groups involved in stabilization and capping of these biogenic nanoparticles [42].

HCT 116 cells, among the three cancer cell types tested in the present study, exhibited the highest sensitivity to MZLAgNPs with the lowest IC₅₀ value in a time and dose-

Fig. 13 Western blot analysis of apoptosis-related protein expression of PARP (active) and caspase-3 (active) in HCT 116 cells treated with MZLAgNPs/cisplatin (control, 10 $\mu\text{g}/\text{mL}$, 25 $\mu\text{g}/\text{mL}$, 50 $\mu\text{g}/\text{mL}$ and cisplatin (16 $\mu\text{g}/\text{mL}$). Data shown as mean \pm SD of three independent experiments



dependent manner. This is in agreement with previous studies on different cancer cell-type specific cytotoxic responses against nanoparticles of defined sizes and exposure time [43–45] barring a few on lymphocytes and erythrocytes [46, 47]. Given the fact that interaction of NPs with erythrocyte is biologically relevant, our results of hemolytic assay reveal the hemocompatibility of MZLAgNPs for drug delivery applications. It is relevant to note that while reporting inhibition of Ehrlich ascites carcinoma in mice by ethyl acetate extract of *M. sapota* leaf, Rashid et al. (2014) had also observed hematoprotective activity against both lymphocytes and erythrocytes. Interestingly, the anticancer effects of MZLAgNPs were clearly evident against HCT 116; human lymphocytes and erythrocytes remained apparently unaffected and normal bereft of any cellular changes. Light, scanning and fluorescence microscopy of cells treated with MZLAgNPs confirmed cytomorphological alterations associated with apoptosis induction in addition to dose-dependent loss of ability to migrate and form colonies. Genotoxic effects of biogenic silver nanoparticles were also confirmed as evidenced by observation of

DNA strand breaks in the form of diffuse comet tails as reported previously [34].

RTq-PCR is one of the most sensitive techniques for detection and quantification of specific mRNAs and/or identification of patterns of gene expression in cells. Expression levels of apoptosis-related genes such as p53-upregulated modulator of apoptosis (PUMA), caspase-3, caspase-8, caspase-9, Bcl-2, and Bax were also determined for studying biogenic MZLAgNP-induced changes in the transcriptional profiles of HCT 116 cells. Gene-specific transcript profiling by RTqPCR in the present study revealed that MZLAgNPs treatment significantly elevated expression of pro-apoptotic genes PUMA, caspase-3 and caspase-8 compared to the expression elicited following exposure to the anticancer drug cisplatin. Notably, at concentrations beyond IC_{50} , caspase-8 and PUMA downregulation was observed as reported earlier [48]. Biogenic AgNPs have also been reported to stimulate PUMA expression in colon cancer through Bax in a mitochondria-dependent manner [13, 37]. Likewise, silver nanoparticle treatment also resulted in increased expression

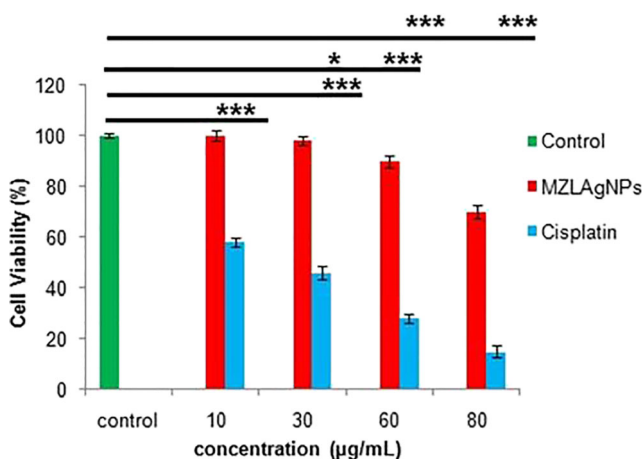


Fig. 14 Effect of MZLAgNPs/cisplatin on normal human hPBLs cells assessed by MTT method. Values represent mean \pm SD of three experiments (** $P \leq 0.01$, ** $P \leq 0.01$, * $P \leq 0.05$)

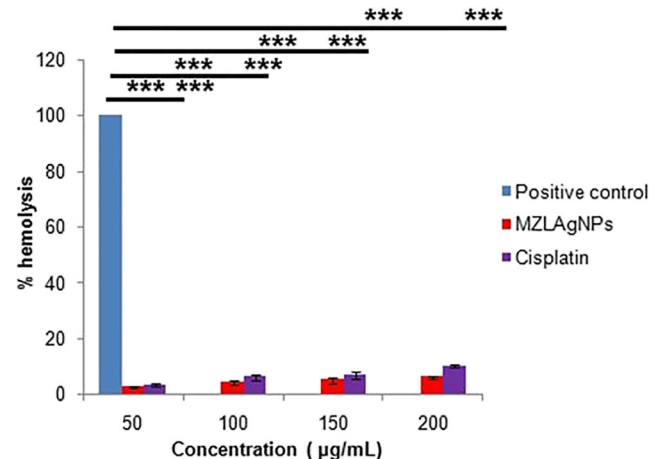


Fig. 15 Cytotoxicity evaluation of biogenic AgNPs/cisplatin against human erythrocytes. Toxicity was measured as percentage hemolysis. Values represent mean \pm SD of three experiments (** $P \leq 0.001$)

of caspase-3 and caspase-8 in A549 NSCLC cells [49]. Downregulation of Bcl-2 and upregulation of Bax following treatment with MZLAGNP/cisplatin was also observed.

Apoptosis is believed to be one of the major consequences of anticancer drug treatment against malignancies. Caspase-3 is a key executioner of apoptosis. PARP, a nuclear enzyme involved in the repair of damaged DNA [50], is inactivated following cleavage by caspase-3 during apoptotic induction. The presence of hallmark proteins, caspase-3 and cleaved PARP, as evidenced by the results obtained by us on western blots, confirm mitochondria-mediated intrinsic pathway of apoptosis induction. Incidentally, expression levels were not proportionate to the transcript levels as revealed by RTq-PCR data. Interestingly, similar to our observations, interaction of 20 nm AgNPs with human neutrophils has been reported to induce apoptosis along with potent inhibition of de novo protein synthesis [51].

In conclusion, the present study has successfully demonstrated that biogenic MZLAGNPs exhibit potent cytotoxicity against colorectal carcinoma cells along with effective inhibition of cell migratory abilities. They were also found to induce cell cycle arrest and mitochondria-mediated apoptosis and thus possess therapeutic potential. The fact that these particles failed to display any deleterious effect on normal hPBLs/RBCs, attests to their biosafety against normal human cells.

Acknowledgements The authors would like to thank the National Institute of Technology, Calicut, for use of SEM and EDX facility. Thanks are also due to our sister departments of Chemistry and Physics and Central Sophisticated Instruments Facility, University of Calicut, for allowing use of facilities to carry out FTIR, XRD, and SEM analysis and Rajiv Gandhi Centre for Biotechnology, Thiruvananthapuram for allowing use of their FACS facility. VSS acknowledges technical help by Jobish Joseph with the figures.

Funding Information This study received financial support from Calicut University by way of Research fellowship to VSS.

Compliance with Ethical Standards

Ethical Statement The blood samples used for hemolysis assay and isolation of lymphocytes for lymphocyte culture and MTT assay was willingly self-donated by the first author (Shaniba V.S.) and the second author (Ahlam Abdul Aziz) of the manuscript submitted. It may be noted that according to the Indian Council for Medical Research, New Delhi, India, Chapter-II, page no. 11–12, the ethical approval for this research was not deemed to be necessary. According to this guideline, proposals which present less than minimal risks are exempted from the ethical review process.

Conflict of Interest The authors declare that there is no conflict of interests.

Publisher's Note Springer Nature remains neutral with regard to jurisdictional claims in published maps and institutional affiliations.

References

1. Anjum S, Haider BA, Khan ZS (2016) Plant mediated synthesis of silver nanoparticles for biomedical applications: challenges and opportunities. *Park J Bot* 48(4):1731–1760
2. Song JY, Kim BS (2009) Rapid biological synthesis of silver nanoparticles using plant leaf extracts. *Bioprocess Biosyst Eng* 32:79–84
3. Rajasekharreddy P, Rani PU, Sreedhar B (2010) Qualitative assessment of silver and gold nanoparticle synthesis in various plants: a photobiological approach. *J Nanopart Res* 12:1711–1721
4. Huang H, Yang X (2004) Synthesis of polysaccharide-stabilized gold and silver nanoparticles. A green method. *Carbohydr Res* 339:2627–2631
5. Xue B, He D, Gao S, Wang D, Yokoyama K, Wang L (2016) Biosynthesis of silver nanoparticles by the fungus *Arthroderma fulvum* and its antifungal activity against genera of *Candida*, *Aspergillus* and *Fusarium*. *Int J Nanomedicine* 11:1899–1906
6. Shankar SS, Rai A, Ahmad A, Sastry M (2004) Rapid synthesis of Au, Ag, and bimetallic Au core–Ag shell nanoparticles using neem (*Azadirachta indica*) leaf broth. *J Colloid Interface Sci* 275:496–450
7. Ahmed S, Ahmad M, Lal BS, Ikram S (2016) A plants extracts mediated synthesis of silver nanoparticles for antimicrobial applications: a green expertise. *J Adv Res* 7:17–28
8. Salunke BK, Sawant SS, Lee S-I, Kim BS (2016) Microorganisms as efficient biosystem for the synthesis of metal nanoparticles. Current scenario and future possibilities. *World J Microbiol Biotechnol* 32(5):1–16
9. Barabadi H, Ovais M, Khan ZH, Saravanan M (2017) Anti-cancer green bionanomaterials: present status and future prospects. *Green Chem Lett Rev* 10(4):285–314
10. Khatoon N, Ahmed JM, Sardar M (2017) Biotechnological applications of green synthesized silver nanoparticles. *J Nanosci Curr Res* 2:1. <https://doi.org/10.4172/2572-0813.1000107>
11. Xi Feng Z, Wei S, Sangiliyandi G (2016) Silver nanoparticles-mediated cellular responses in various cell lines: an in vitro model. *Int J Mol Sci* 17(10):1603–1629
12. Ovais M, Khalil AT, Raza A, Khan MA, Ahmad I, Islam NU, Saravanan M, Ubaid MF, Ali M, Shinwari ZK (2016) Synthesis of silver nanoparticles via plant extracts: beginning a new era in cancer theranostics. *Nanomedicine* 11(23):3157–3177
13. Kovacs D, Igaz N, Keskeny C, Bélteky P, Tóth T, Gáspár R, Madarász D, Rázga Z, Kónya Z, Imre, Boros M, Kiricsi M (2016) Silver nanoparticles defeat p53-positive and p53-negative osteosarcoma cells by triggering mitochondrial stress and apoptosis. *Sci Rep* 6:27902. <https://doi.org/10.1038/srep27902>
14. Hackenberg S, Scherzed A, Kessler M, Hummel S, Technau A, Froelich K, Ginzkey C, Koehler C, Hagen R, Kleinsasser N (2011) Silver nanoparticles: evaluation of DNA damage, toxicity and functional impairment in human mesenchymal stem cells. *Toxicol Lett* 201(1):27–33
15. Banerjee D, Sengupta S (2011) Nanoparticles in cancer chemotherapy. *Prog Mol Biol Transl Sci* 104:489–507
16. Ranganathan R, Madanmohan S, Kesavan A, Baskar G, Ramia Y, Krishnamoorthy, Santosham R, Ponraju D, Kumar SR, Venkatraman G (2012) Nanomedicine: towards development of patient-friendly drug-delivery systems for oncological applications. *Int J Nanomedicine* 7:1043–1060
17. Milind P, Preeti (2015) Chickoo: a wonderful gift from nature. *Int J Res Ayurveda Pharm* 6(4):544–555
18. Ghani A (2003) Medicinal plants of Bangladesh: chemical constituents and uses, 2nd edn. Asiatic Society of Bangladesh, Dhaka, p 292

19. Kulkarni AP, Policegoudra RS, Aradhya SM (2007) Chemical composition and antioxidant activity of Sapota (*Achras sapota* Linn.) fruit. *J Food Biochem* 31:399–414
20. Priya P, Shoba FG, Parimala M, Sathya J (2014) Antioxidant and antibacterial properties of *Manilkara zapota* (L.) Royen flower. *Int J Pharm Clin Res* 6(2):174–178
21. Anjaria J, Parabia M, Dwivedi S (2002) Ethnovete heritage Indian ethnoveterinary medicine, an overview. Pathik Enterprise, Ahmedabad
22. Patricia LDM, Maria RAM, Luis COL, Jose DA, Ricardo EA, Jose DS (2008) Cell wall biochemistry of sapodilla (*Manilkara zapota*) submitted to 1-methylcyclopropene. *Braz J Plant Physiol* 20:85–94
23. Anand P, Kulkarni RS, Policegoudra S, Aradhya M (2007) Chemical composition and antioxidant activity of sapota (*Achras sapota* Linn.) fruit. *J Food Biochem* 31:399–414
24. Bhargava KP, Gupta M, Gupta GP, Mitra CR (1970) Anti-inflammatory activity of saponins and other natural products. *Indian J Med Res* 58:724–730
25. RB et al (1979) Steroid and triterpenoid saponins as spermicidal agents. *Indian Drugs* 17: 6–8
26. Ma J, Luo XD, Protiva P, Yang H, Ma C, Basile MJ, Weinstein B, Kennelly EJ (2003) Bioactive novel polyphenols from the fruit of *Manilkara zapota* (sapodilla). *J Nat Prod* 66:983–986
27. Fayek NM, Monem ARA, Mossa MY, Meselhy MR, Shazly AH (2012) Chemical and biological study of *Manilkara zapota* (L.) Van Royen leaves (Sapotaceae) cultivated in Egypt. *Pharm Res* 4:85–91
28. Rashid MM, Hossain MI, Osman MA, Aziz MA, Habib MR, Karim MR (2014) Evaluation of antitumor activity of *Manilkara zapota* leaves against Ehrlich ascites carcinoma in mice. *Environ Exp Biol* 12:131–135
29. Srivastava M, Hegde M, Chiruvella KK, Koroth J, Bhattacharya S, Choudhary B, SCR (2014) Sapodilla plum (*Achras sapota*) induces apoptosis in cancer cell lines and inhibits tumor progression in mice. *Sci Rep* 4:6147. <https://doi.org/10.1038/srep06147>
30. Mossmann T (1983) Rapid colorimetric assay for cellular growth and survival: application to proliferation and cytotoxicity assays. *Immunol Methods* 65(1):55–63
31. He Y, Du Z, Ma S, Cheng S, Jiang S, Liu Y, Li D, Huang H, Zhang K, Zheng X (2016) Biosynthesis, antibacterial activity and anticancer effects against prostate cancer (PC-3) cells of silver nanoparticles using *Dimocarpus Longan Lour.* Peel extract. *Nanoscale Res Lett* 11:300. <https://doi.org/10.1186/s11671-016-1511-9>
32. Franken NAP, Rodermond HM, Stap J, Haveman J, van Bree C (2006) Clonogenic assay of cells in vitro. *Nat Protoc* 1:2315–2319
33. Sreekanth D, Arunasree MK, Roy KR, Reddy TC, Reddy GV, Reddanna PV (2007) Betanin a betacyanin pigment purified from fruits of *Opuntia ficus-indica* induces apoptosis in human chronic myeloid leukemia cell line- K562. *Phytomedicine* 14:739–746
34. Singh NP, McCoy MT, Tice RR, Schneider EL (1988) A simple technique for quantitation of low levels of DNA damage in individual cells. *Exp Cell Res* 175:184–191
35. Jeyaraj M, Sathishkumar G, Sivanandhan G, MubarakAli D, Rajesh M, Arun R, Kapildev G, Manickavasagam M, Thajuddin N, Premkumar K, Ganapathi A (2013) Biogenic silver nanoparticles for cancer treatment: an experimental report. *Colloids Surf B* 106: 86–92
36. Zhen X, Cen J, Li YM, Yan F, Guan T, Tang XZ (2011) Cytotoxic effect and apoptotic mechanism of tanshinone A, a novel tanshinone derivative, on human erythroleukemic K562 cells. *Eur J Pharmacol* 667:129–135
37. Kuppusamy P, Ichwan SJA, Nur PHA, Hidayati WS, Soundharajan I, Govindan N, Pragas GM, Mashitah MY (2016) In vitro anticancer activity of Au, Ag nanoparticles synthesized using *Commelina nudiflora* L. Aqueous extracts against HCT 116 colon cancer cells. *Biol Trace Elem Res* 173:297–305
38. Ausubel FM, Brent R, Kingston RE, Moore DD, Seidman J, Smith JA, Struhl K (1992) Short protocols in molecular biology. Wiley, USA, pp 10.8.1–10.8.23
39. Khan M, Naqvi AH, Ahmad M (2015) Comparative study of the cytotoxic and genotoxic potentials of zinc oxide and titanium dioxide nanoparticles. *Toxicol Rep* 2:765–774
40. Buttacavoli M, Ninfa NA, Di Cara J, Alduina R, Faleri C, Gallo M, Pizzolanti G, Gallo G, Feo S, Baldi F, Cancemi P (2018) Anticancer activity of biogenerated silver nanoparticles: an integrated proteomic investigation. *Oncotarget* 9:9685–9705
41. Krishnaraj C, Jagan EG, Rajasekar S, Selvakumar P, Kalaihelvan PT, Mohan N (2010) Synthesis of silver nanoparticles using *Acalypha indica* leaf extracts and its antibacterial activity against water borne pathogens. *Colloids Surf B* 76:50–56
42. Dipankar C, Murugan S (2012) The green synthesis, characterization and evaluation of the biological activities of silver nanoparticles synthesized from *Iresine herbstii* leaf aqueous extracts. *Colloids Surf B* 98:112–119
43. Gurunathan S, Han JW, Eppakayala V, Jeyaraj M, Kim JH (2013) Cytotoxicity of biologically synthesized silver nanoparticles in MDA-MB-231 human breast cancer cell. *Biomed Res Int*. <https://doi.org/10.1155/2013/535796>
44. Vasanth K, Ilango K, MohanKumar R, Agrawal A, Prasad GD (2014) Anticancer activity of Moringa oleifera mediated silver nanoparticles on human cervical carcinoma cells by apoptosis induction. *Colloids Surf B* 117:354–359
45. Zhu B, Li Y, Lin Z, Zhao M, Xu T, Wang C, Deng N (2016) Silver nanoparticles induce HePG-2 cells apoptosis through ROS-mediated signaling pathways. *Nanoscale Res Lett* 11:198. <https://doi.org/10.1186/s11671-016-1419-4>
46. Vergallo C, Panzarini E, Izzo D, Carata E, Mariano S, Buccolieri A, Serra A, Manno D, Dini L (2014) Cytotoxicity of β -D-glucose coated silver nanoparticles on human lymphocytes. *AIP Conf Proc* 1603:78–85
47. Bhanumathi R, Vimala K, Shanthi K, Thangaraj R, Kannan S (2017) Bioformulation of silver nanoparticles as berberine carrier cum anticancer agent against breast cancer. *New J Chem* 41:14466–14477
48. Abbasi AK, Hamid SZ, Bordbar A, Reza AK, Razmjou A, Kardi M (2016) Anticancer effects of silver nanoparticles encapsulated by *Taxus baccata* extracts. *J Mol Liq* 223:549–556
49. Karthik S, Sankar R, Varunkumar K, Ravikumar V (2014) Romidepsin induces cell cycle arrest, apoptosis, histone hyperacetylation and reduces matrix metalloproteinases 2 and 9 expression in bortezomib sensitized non-small cell lung cancer cells. *Biomed Pharmacother* 68:327–334
50. D'Amours D, Desnoyers S, D'Silva I, Poirier GG (1999) Poly (ADPribose)ylation reactions in the regulation of nuclear functions. *Biochem J* 342:249–268
51. Poirier M, Simard J, Antoine F, Girard D (2014) Interaction between silver nanoparticles of 20 nm ($AgNP_{20}$) and human neutrophils: induction of apoptosis and inhibition of *de novo* protein synthesis by $AgNP_{20}$ aggregates. *J Appl Toxicol* 34:404–412